Environment International 168 (2022) 107484

Contents lists available at ScienceDirect

Environment International

journal homepage: www.elsevier.com/locate/envint

Full length article

Rice hull biochar enhances the mobilization and methylation of mercury in a soil under changing redox conditions: Implication for Hg risks management in paddy fields

Ying Xing [a,b], Jianxu Wang [c,b,1], Christoph E.S. Kinder [b], Xing Yang [b], Michal Slaný [d], Bing Wang [e], Hocheol Song [f], Sabry M. Shaheen [b,g,h], Peter Leinweber [i,j], Jörg Rinklebe [b,f,*]

[a] School of Chemistry and Materials Science, Guizhou Normal University, Guiyang 550002, PR China
[b] University of Wuppertal, School of Architecture and Civil Engineering, Institute of Foundation Engineering, Water- and Waste-Management, Laboratory of Soil- and Groundwater-Management, Pauluskirchstraße 7, 42285 Wuppertal, Germany
[c] State Key Laboratory of Environmental Geochemistry, Institute of Geochemistry, Chinese Academy of Sciences, Guiyang 550082, PR China
[d] Institute of Inorganic Chemistry, Slovak Academy of Sciences, Dúbravská cesta 9, 845 36 Bratislava, Slovakia
[e] College of Resources and Environment Engineering, Guizhou University, Guiyang, Guizhou 550025, PR China
[f] University of Sejong, Department of Environment, Energy and Geoinformatics, 98 Gunja-Dong, Guangjin-Gu, Seoul, South Korea
[g] King Abdulaziz University, Faculty of Meteorology, Environment and Arid Land Agriculture, Department of Arid Land Agriculture, Jeddah 21589, Saudi Arabia
[h] University of Kafrelsheikh, Faculty of Agriculture, Department of Soil and Water Sciences, 33516 Kafr El-Sheikh, Egypt
[i] University of Rostock, Department Light, Life and Matter (LLM), Albert-Einstein-Strasse 25, D-18059 Rostock, Germany
[j] Soil Science, University of Rostock, Justus-von-Liebig-Weg 6, 18051 Rostock, Germany

ARTICLE INFO

Handling Editor: Adrian Covaci

Keywords:
Hg methylation
Redox chemistry
Paddy soil
Soil organic matter composition
Mercury mine

ABSTRACT

Biochar amendment to paddy soils was promising to mitigate mercury (Hg) accumulation in rice; thus, it was applied to reduce human Hg exposure via rice consumption. However, how biochar affects Hg mobilization and MeHg formation in soil under changed redox potential (E_h) conditions remained unknown. Here, we explored the change of dissolved total Hg (DTHg) and dissolved MeHg (DMeHg), and their controlling biogeochemical factors in a soil with(out) biochar amendment under changing E_h conditions using biogeochemical microcosm. Biochar amendment resulted in a widen E_h range (−300 to 400 mV) compared to the control (−250 to 350 mV), demonstrating that biochar promoted reduction-oxidization reactions in soil. Biochar amendment enhanced Hg mobilization by mediating reductive dissolution of Fe/Mn (hydr)oxides. Thus, the increased Hg availability promoted MeHg formation in the soils. Biochar amendment changed the soil organic matter (SOM) composition. Positive correlations between the relative abundance of LIPID (lipids, alkanes/alkenes), ALKYL (alkylaromatics), and suberin and MeHg concentrations indicate that these SOM groups might be related to MeHg formation. Biochar enhanced the releasing and methylation of Hg by promoting the mobilization of Fe(oxyhydr)oxides and alternation of carbon chemistry under dynamic E_h conditions. There is an unexpected environmental risk associated with biochar application to paddy soils under dynamic E_h condition, and one should be aware this risk when applying biochar aiming to minimize human Hg exposure health risks via rice consumption.

1. Introduction

Mercury is toxic to human, and the long-range transport of elemental gas Hg in the atmosphere can cause contamination of remote land via deposition (Hsu-Kim et al., 2018; Beckers and Rinklebe, 2017). Mercury released from both natural and human activities has contaminated soils, causing Hg bioaccumulation in food chain (Wang et al., 2012, 2016). Human exposure to Hg through consumption of crops cultivated at Hg-contaminated farmlands (Liu et al., 2019; Wang et al., 2020). Consumption of Hg-contaminated foods is the major pathway of human exposure to both MeHg and inorganic Hg at Hg-contaminated regions worldwide (Feng et al., 2008; Li et al., 2015). Therefore, urgent

* Corresponding author at: University of Wuppertal, School of Architecture and Civil Engineering, Institute of Foundation Engineering, Water- and Waste-Management, Laboratory of Soil- and Groundwater-Management, Pauluskirchstraße 7, 42285 Wuppertal, Germany.
E-mail addresses: wangjianxu@vip.gyig.ac.cn (J. Wang), rinklebe@uni-wuppertal.de (J. Rinklebe).
[1] Co-corresponding author.

https://doi.org/10.1016/j.envint.2022.107484
Received 16 May 2022; Received in revised form 16 August 2022; Accepted 18 August 2022
Available online 24 August 2022

measures and actions are needed to reduce the concentration of Hg in crops (Zhao et al., 2015), and thereby reducing human Hg exposure health risks. Remediation methods for farmlands are sparse (Wang et al., 2019a, 2020), and those for industrial contaminated sites (e.g., stabilization/solidification, thermal treatment, and vitrification) are often destructive, costly, and environmental-unfriendly (Wang et al., 2012). The reduction of bioavailability of pollutants by addition of amendments (*in-situ* immobilization) has attracted global interests because it is *in-situ*, easy to manage and environment-friendly (Palansooriya et al., 2020; Wang et al., 2019a,b; Wu et al., 2021). Developing commercial and cost-effective amendments is crucial for establishing successful *in-situ* immobilization methods (Porter et al., 2004; Yang et al., 2022).

Biochar produced from pyrolysis of biomass under O_2-limitation (Bolan et al., 2022; Joseph et al., 2021) is a popular soil amendment due to its great potentiality in improving soil quality, and carbon sequestration against global warming (Rinklebe et al., 2016;Shaheen et al., 2022a,b). Biochar can serve as an electron donator and acceptor, and transfer electrons to promote reduction and oxidization of redox-sensitive elements (Lau et al., 2015; Amen et al., 2020). Enhanced redox reactions by biochar likely affect Fe/Mn(hydr)oxides and carbon chemistry, which in turn influence the speciation of trace elements (Awad et al., 2018; Liu et al., 2019a). There is a growing interest of using biochar to mitigate Hg risks from paddy soils because both, pot and field experiments had demonstrated that biochar amendment could reduce the concentration of Hg in rice grain (Xing et al., 2019, 2020; Shaheen et al., 2022a). For example, Xing et al. (2020) performed a field trial to study the amendment of 24–72 t ha^{-1} rice hull biochar to paddy soils on Hg accumulation by rice grain, and results showed that total Hg and MeHg content decreased by 32–36 % and 47–53 %, respectively, as compared to non-treated control. Mechanisms of Hg decrease in rice plants by biochar are often attributed to the inhibition of MeHg formation or a decreased bioavailability of MeHg in paddy soils (Shu et al., 2016; Xing et al., 2020). However, the performance of biochar on the mobilization and methylation of Hg in paddy soils under varied environmentally-relevant redox conditions is largely unknown. A pilot study from Beckers et al. (2019) showed that Hg mobilization was poorly affected by pine cone biochar in a contaminated floodplain soil under changed redox potential (E_h) conditions.

Biochar can change pH and the composition of dissolved organic matter (DOM) in soils (Cooper et al., 2020; Jing et al., 2020). The change of pH can cause desorption of DOM from mineral phases. Also, biochar can preferentially sorb DOM with high aliphaticity (Smebye et al., 2016). Organic matter compositions play a vital role for the formation of MeHg (Bravo et al., 2017; Jiang et al., 2018; Knorr and Blodau, 2009). For example, low-mass thiol-containing molecules can facilitate bacteria-mediated Hg methylation (Schaefer et al., 2011). Nevertheless, the change of organic matter composition by biochar and how this change affects Hg mobilization and methylation in soils under dynamic redox conditions is still unclear.

The Wanshan Hg mine is located in the Southwestern part of China, and its historical mining and retorting activities had resulted in severe Hg pollution in surrounding soils (Wang et al., 2011). The Wanshan Hg mine region had been listed as one of six pilot demonstration zones by the Chinese government for Hg remediation (Sun et al., 2020), and rice hull biochar was amended for paddy field remediation (Xing et al., 2019). We collected both a control and a biochar-treated soil from a paddy field at the Wanshan Hg mine. For the first time, we incubated both the control and biochar-treated soils to dynamic redox conditions in automated biogeochemical microcosms. Thereby, we simulated flooding conditions to mimic dynamic changes of the redox potential as it naturally occurs in paddy soils. We aimed to elucidate (1) the impacts of biochar on the Hg mobilization and MeHg formation, (2) how biochar affects biogeochemical factors (e.g., Fe/Mn(hydr)oxides, dissolved organic carbon (DOC), sulfate, etc.), and their associations with Hg mobilization (3) how biochar alters the composition of soil organic matter (SOM), and how these changes affect MeHg formation. The gained results are critical to use biochar as a sustainable amendment to reduce Hg accumulation by rice, and thereby minimizing human health risks through rice consumption.

2. Materials and methods

2.1. Production and characterization of biochar

The rice hulls were pyrolyzed at 550 to 600 °C in low oxygen environment to produce rice hull-derived biochar (Xing et al., 2020). The pH and electric conductivity (EC) were determined according to Xing et al. (2020). The determination of total C, N, and S was performed using a Total C/N analyzer. Carbon functional groups of biochar were revealed using X-ray photoelectron spectroscopy (XPS) (K-Alpha, ThermoFisher, USA), and Raman spectrometry (ARAMIS, HoribaJobin, Japan). Morphology and elemental compositions of biochar were characterized by a scanning electron microscopy (SEM, Hitachi S-4800 with ISIS 310, Japan) coupled with energy-dispersive spectroscopy (EDS).The produced biochar was neutral (pH = 7.1); it had total carbon (C), nitrogen (N) and sulfur (S) content of 530, 7.9, and 0.9 g kg^{-1}, respectively. The total Hg content in the biochar was less than 0.3 mg kg^{-1}.

2.2. Soils collection

Both, non-biochar treated soil (control) and biochar-treated soil (amendment of 72 t ha^{-1} rice hull-derived biochar to the Wanshan soil at a treatment depth of 30 cm) were collected from the experimental farmlands at the Wanshan Hg mining region, China (Xing et al., 2020). The control soil and the biochar-treated soil were collected after aging for 3 months in the field. About 100 kg of top layer soil samples (0–30 cm) were randomly collected from either control or biochar treatment, and thereafter they were sieved (4-mm) after being air-dried. The control soil was neutral (pH = 6.7) and its electric conductivity (EC) was 132 μS cm^{-1}. Total C, N and S concentration in the control soil was 2.5, 0.32 and 0.035 %, respectively. The concentration of total Hg was 39.8 ± 4.9 mg kg^{-1} (n = 3) and MeHg was 2.5 ± 0.2 ng g^{-1} (n = 3). Soil texture was characterized as silt loam: 0.01–2 μm (6 %), 2–20 μm (34 %), and 20–200 μm (59 %). The biochar-treated soil was neutral (pH = 6.56), and its EC value was 120 μS cm^{-1}. Total C, N and S concentration in the biochar-treated soil was 5, 0.35 and 0.036 %, respectively; Total Hg and MeHg concentration was 38 ± 2.6 mg kg^{-1} (n = 3) and 4.3 ± 0.4 ng g^{-1} (n = 3), respectively (Xing et al., 2020).

2.3. Microcosm study

Automated biogeochemical microcosm (MC) equipment was adopted to study the Hg mobilization and MeHg formation under changing redox conditions. The detailed setup information of the MC system is described previously; an image and a schematic of MC equipment are displayed in the Supplementary information (Yu et al., 2007; Yu and Rinklebe, 2011). About 210 g of air-dry soil together with 1680 mL of tap water were filled in each 2 L glass vessel equipped in each microcosm (MC), and then the vessel was air-tight closed. The soil suspension was constantly stirred during the experimental period (28 days). Each treatment had three independent replicated MCs. Both, pH and E_h values of each MC unit were recorded by a data logger every 10 min. The E_h was stepwise regulated by flushing N_2 (decreasing E_h) or synthetics air/O_2 (increasing E_h) to predefined E_h windows −250 mV (−300 mV for the biochar treatment), −200 mV, −100 mV, 0 mV, +100 mV, +200 mV, +350 mV (+400 mV for the biochar treatment), respectively. The soil suspension was kept for 48 h at each pre-set E_h window prior to sampling.

A volume of 80 mL of the soil suspension was collected from each MC at each predefined E_h window using a syringe. Also, a soil suspension sample (initial) was collected at the beginning of the experiment. The soil suspensions were transferred to 50-mL centrifuge tubes in a

anaerobic chamber (glove box) filled with 90 % N_2 and 10 % H_2. Thereafter, samples were centrifuged at 5000 rpm for 15 min. The centrifuged suspension was filtrated through a 0.45-μm pore size membrane filter in an inert atmosphere. Subsequently, the filtrate was divided into five subsamples. The first subsamples were acidified to 1 % with concentrated HNO_3 (65 %) for total Fe and Mn analyses; the second subsample group was acidified to 2 % with concentrated HCl (45 %) for the analysis of both, MeHg and THg; the residual subsamples were analyzed for dissolved organic carbon (DOC), sulfate, and specific UV absorbance ($SUVA_{254}$), respectively. Soils precipitated in the tubes were collected, and freeze-dried for total MeHg analysis.

2.4. Soil solutions analysis

The concentration of dissolved Hg was measured by a DMA-80 Hg analyzer (Milestone Srl, Sorisole, Italy), which has a absolute detection limit of 0.05 ng (Wang et al., 2019a). MeHg concentration in soil solution was determined in accordance with U.S. EPA method 1630 (USEPA, 2001). The concentrations of dissolved Fe and Mn, dissolved organic carbon (DOC), sulfate, and Specific UV light absorbance at 254 nm wavelength ($SUVA_{254}$) were measured according to the standard methods (Supplementary information, S1.1) (Wang et al., 2021; Yang et al, 2022).

2.5. Soil solid phase analysis

MeHg in soil samples was analyzed using the method of Liang et al. (2004). Briefly, soil samples were extracted with the mixture of $CuSO_4$-methanol, and the phase concentrated with MeHg was separated by dichloromethane (CH_2Cl_2). MeHg was determined using a CVAFS analyzer (Brooks Rand Instruments, USA). Carbon *K*-edge X-ray absorption near-edge structure spectroscopy (XANES) analysis was performed for both, the control and biochar-treated soil at the beamline 4B7B at Beijing Synchrotron Radiation Facility. The analytical procedure for XANES was adopted from Wang et al. (2015). The near-IR (NIR) spectra of the control and biochar-treated soil were collected using the Fourier Transform Infrared (FT-IR) spectrometer (Nicolet 6700, Thermo Scientific™).The CaF_2 beam splitter, white light source and InGaAs detector were used for near-IR region (8000–4000 cm^{-1}). Measurement setting was 64 scans with a resolution of 4 cm^{-1} and spectra manipulation was performed according to the method of Slaný et al. (2022). Organic matter composition of soil was determined by Pyrolysis–Field Ionization Mass Spectrometry (Py-FIMS). The Py-FIMS methodology, including type of instrument, high vacuum conditions, heating rate, and ion detection was described previously (Schulten and Leinweber, 1999; Shaheen et al., 2022b). Assignment of marker signals (m/z) to relevant compound classes was shown in Table S1 (Leinweber et al., 2009).

2.6. Data quality control/quality assurance

The controlling of data quality was achieved by quadruplicate/triplicate analyses, blank samples, and employment of standard solutions (Merck) during the measurement. The acceptable value was defined as relative standard deviation (RSD) between replicates of lower than 15 %. Certified soil reference materials named GBW(E)070009 and CC580 obtained from the Institute of Geophysical and Geochemical Exploration, China were utilized for quality assurance of Hg analysis. The recovery ratios for total Hg and MeHg are presented in Table S2. The IBM SPSS Statistics 23 (NY, USA) was used for statistical analyses. One-way ANOVA was used to test means for the variables with Duncan's multiple range tests at $P < 0.05$. Figures were created using OriginPro 9.1 b215 (OriginLab Corporation, Northampton, USA). Multivariate regression analyses were performed using Microsoft Office Excel 2010.

3. Results and discussion

3.1. Chemical composition and morphology of the studied rice hull biochar

The high-resolution spectrum of the carbon region using XPS of the studied biochar showed the three deconvoluted peaks of C 1s at 284.3, 285.4, and 287.5 eV, respectively (Fig. 1-A). They correspond to sp^2-hybridized carbon (284.3 eV), C—O/C—OH (285.4 eV), and carbonyl groups (287.5 eV) (Kim et al., 2015; Sorrenti et al., 2016).The Raman spectrum of the biochar has a peak at 1580 cm^{-1} reflecting a sp^2-hybridized graphitic carbon structure (G-band), and another peak at 1357 cm^{-1} (Fig. 1-B), indicating in-plane vibrations of sp^2-type carbon within structural defects (D band) (Fang et al., 2017; Maghsoumi et al., 2015). Thus, both, the XPS and Raman spectra, provided a clear evidence of the high aromatic structure of the studied rice hull-derived biochar. This agreed with an earlier study (Xiao et al., 2018).

The SEM image showed an irregular and rough surface of the biochar particles (Fig. S1). The EDX spectroscopic analysis revealed that biochar particles contained 53 % C, 0.1 % Na, 0.1 % Mg, 4.0 % Si, 0.63 % K, and 1.0 % Ca, respectively. Carbon content obtained by EDX spectroscopy (53 %) matched well with the results obtained by total C/N analyzer (53 %) (S1.2, supplementary information), demonstrating that the particles for SEM-EDX analysis were representative for the bulk of biochar matter. The studied biochar contained more Si (4 %) than Ca (1.0 %), K (0.63 %), Na (0.1 %), and Mg (0.1 %) (Fig. S1), as rice hull was rich in Si (Savant et al., 1996).

3.2. Carbon content and its functional groups in the soils

The content of total carbon in the biochar treatment (total carbon content = 5 %) was 2 times higher than in the control (total carbon content = 2.5 %), which is related to the input of carbon originating from the biochar (Xing et al., 2019). The carbon *K*-edge XANES spectra of both, the control and the biochar-treated soil show two clear peaks at 285.4 and 288.9 eV (Fig. 1-C), corresponding to aromatic (e.g., protonated or alkylated aromatic C) and carboxyl C (e.g., carboxylic, carboxylamide, carbonyl C), respectively (Guo and Chen, 2014; Prietzel et al., 2018). The peak at 285.4 eV is much stronger in the biochar-treated soil as relative to the control, indicating the presence of more aromatic C in the biochar-treated soil, which is consistent with the Raman result (Fig. 1-A, B).

The NIR spectra of the control and biochar-treated soil are shown in Fig. 1-D. The complex band in the region 7150–7000 cm^{-1} is related to the overlapping first overtones of the stretching vibrations of the structural —OH groups of soil and H_2O molecules involved into H-bonds. The absorption band at 5232 cm^{-1} corresponded to the combination ($\nu + \delta$)H_2O band in the soils. The band at 4526 cm^{-1} was observed due to the combination mode of structural OH groups (Slaný et al., 2019). Very weak ($\nu + \delta$)CH bending bands are observed at both 4444 cm^{-1} and 4252 cm^{-1}. The presence of —CH_3 group might come from aromatic carbon (C—O—CH_3 group) (Schmidt-Rohr et al., 2004).

3.3. E_h and pH

The maximum, minimum, and mean values of E_h (6 h before sampling, $n = 1176$) are 334, −219, 62 mV in the control, and 391, −271, 68 mV in the biochar treatment (Fig. 2 and Table S3). The E_h zones of the biochar-treated soil is 109 mV larger than that of the control across the study (Fig. 2 and Fig. S2), which was likely due to the biochar-enhanced redox reactions, as biochar was able to donate via phenolic groups and accept electrons via quinones/polycondensed aromatic structures (Klüpfel et al., 2014; Steinbeiss et al., 2009). Also, biochar could induce interspecies electrons transfer via conduction-based mechanisms (Bourke et al., 2007; Chen et al., 2014; Dissanayake et al., 2018). The studied rice hull biochar was rich in aromatic C and graphitic structures

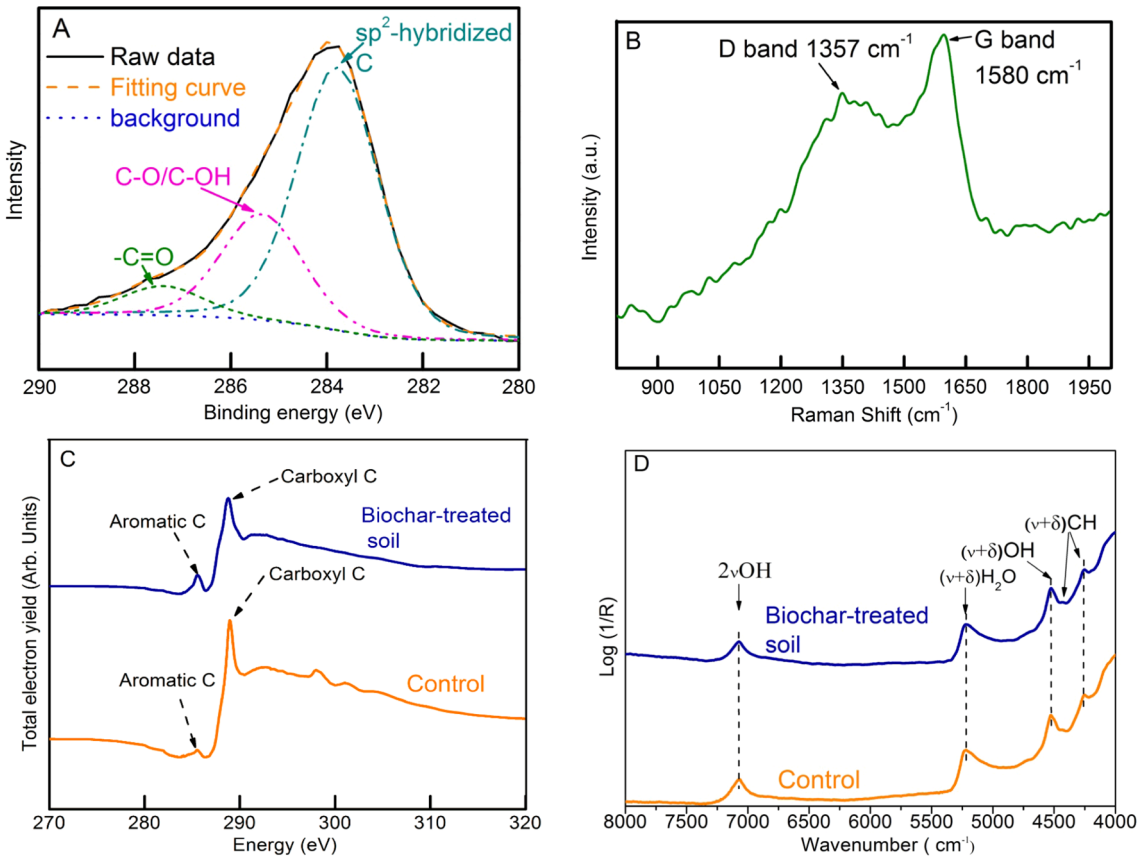

Fig. 1. A: X-ray photoelectron spectrum of the biochar; B: Raman spectrum of the biochar; C: Carbon *K*-edge spectra of control (blue solid line) and biochar-treated soil (Olive solid line); 1s → Π* at 285.4 eV is aromatic carbon, 1s → Π^*_{COOH} at 288.9 eV is carboxyl C; D: NIR spectra (8000–4000 cm^{-1}) of the control and biochar-treated soil.

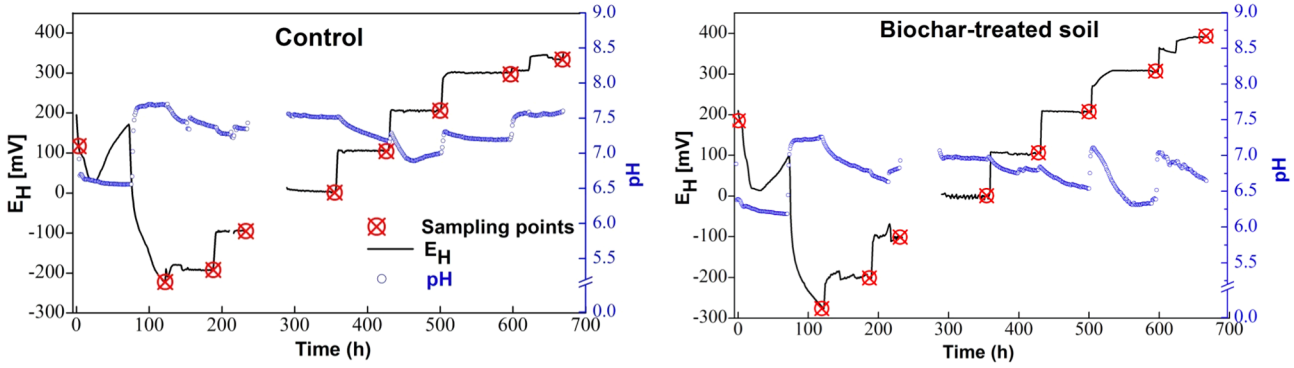

Fig. 2. pH-E_h plots for both control (Left) and biochar-treated soil (Right). The black solid line and blue dash lines are for E_h and pH, respectively. The red crosses on the E_h curve indicates a soil suspension sample was taken at that E_h window. There was a gap in both pH and E_h curves starting from incubation time of 234 min to 288 min in the two plots. This gap was due to the exclusion of the varied pH and E_h values during setup of the pre-defined E_h windows. Note: the pH and Eh values are the average from the three replicates.

(sp^2-hybridized C, Fig. 1-A), which might enhance redox reactions by increasing electron accepting moieties and conductivity in the soil.

The maximum, minimum, and mean values of pH (6 h before sampling, $n = 1176$) were 7.69, 7.00, 7.29 in the control and 7.25, 6.39, 6.73 in the biochar-treated soil (Fig. 2 and Table S3).The pH behave controversially to E_h in the two soils during the change of E_h (Fig. 2 and Fig. S2), which might be related to the depletion of protons by reduction of Fe^{3+}, NO_3^-, and Mn^{4+} under anaerobic conditions, and the release of protons by oxidation processes under aerobic conditions (Rinklebe et al., 2016). The mean pH value in the biochar treatment is 0.63 units lower than the control (Table S3). The studied biochar (pH = 7.09) is more alkaline than the soil (pH = 6.7), and thus, the acidification by biochar was unlikely. Alternatively, microbial-mediated decomposition of small organic molecules of biochar might produce organic acids and CO_2, leading to acidification (Cheng et al., 2017; Yuan et al., 2017). The widened E_h range and decreased pH of the soil suspension, induced by the amendment of biochar should have affected the Hg mobilization and MeHg formation through mediating redox/pH-sensitive reactions.

3.4. Dissolved total Hg (DTHg)

The concentration of DTHg showed an E_h-dependent behavior in

both, control and biochar treated-soils (Figs. 2, 3). In control soil, DTHg concentrations are 0.55–0.91 ng mL^{-1} at the E_h range of −250 to −100 mV, and 0.08–0.34 ng mL^{-1} at the E_h range of 0 to +350 mV (Fig. 3). In the biochar-treated soil, DTHg concentrations are 0.9–1.25 ng mL^{-1} at the E_h range of −300 to −100 mV, and 0.23–1.18 ng mL^{-1} at the E_h range of 0 to +400 mV (Fig. 3). We further compared the concentrations of DTHg between the control and biochar treatment at each E_h window, and found that DTHg concentrations were 29–268 % higher in the biochar treatment relative to control across the studied E_h zones, and the magnitude of increase was smaller at higher E_h ranges (0 mV to +400 mV, 29–64 %) than at lower ranges (−300 mV to −100 mV, 82–268 %) (Fig. 3). The concentration of DTHg in the biochar-treated soil exceeds that in the control. Mercury was mobilized at low E_h, but it was immobilized at high E_h in the two soils. Those results demonstrate that the amendment of the rice hull-derived biochar enhanced the mobilization of Hg under the experimental conditions. To elucidate the biogeochemical processes controlling Hg mobilization, we further studied biogeochemical factors and their geochemical associations with Hg.

3.5. Biogeochemical factors controlling the mobilization of Hg

3.5.1. Fe/Mn redox chemistry

The concentrations of dissolved Fe and Mn varied as a function of E_h in the two treatments (Fig. 3). The concentrations of dissolved Fe and Mn were higher at lower E_h range (−300 to −200 mV), while they decreased when E_h exceeded −100 mV. The formation of Fe/Mn(hydr) oxides from anaerobic to aerobic conditions seemed the dominating biogeochemical process here. Supporting this assumption, we observed significant negative correlations between E_h and Fe/Mn (Fig. S3). The reductive dissolution of Fe/Mn (hydr)oxides led to higher Fe and Mn concentrations in the lower E_h range (−300 to 0 mV). Goethite (α-FeOOH) reduction to Fe^{2+} is initiated at E_h lower than −250 mV, and amorphous Fe(hydr)oxides reduction occurs at E_h −100 mV (Borch et al., 2010). The lowest E_h in the control and biochar treatment was −223 and −277 mV, respectively (Table S3). Under such E_h conditions, we expected an intensive reduction of Fe/Mn oxides (e.g., amorphous Fe oxides, goethite), particularly in the biochar treatment because its E_h was lower (Fig. 2). Overall, the concentrations of dissolved Fe and Mn decreased gradually with the rising of E_h (Fig. 3), because the reductive dissolution of Fe/Mn oxides became weaker and the formation of (hydr) oxides of Fe and Mn was prevalent under higher E_h conditions. Additionally we found significant linear relationships between dissolved Fe/Mn and Hg for the two soils ($P < 0.05$, Fig. 4). The linear correlation coefficient of Hg *vs* Fe (control: $R^2 = 0.90$; biochar: $R^2 = 0.86$) was stronger than that of Hg *vs* Mn (control: $R^2 = 0.37$; biochar: $R^2 = 0.73$) (Fig. 4), which indicates a closer geochemical association of Hg with Fe than that with Mn in the soils (Wang et al., 2021b). The result was consistent with a previous study that Fe oxy(hydr)oxides were important Hg sinks, and Hg had a close geochemical relation with Fe (Harris-Hellal et al., 2011). Consequently, Hg mobilization at low E_h windows shall be closely related to the reductive dissolution of Fe(hydr)oxides. This phenomenon had already been reported in wetlands soils (Frohne et al., 2012). Here, the acidic dissolution of Fe(hydr)oxides was of minor importance because the soil was alkaline (pH > 7.0) at low E_h (Fig. 2).

The average concentrations of dissolved Fe and Mn in the biochar-treated soil were 1.9 and 2.6 times higher than the control soil. The increased concentrations of dissolved Fe and Mn might partially originate from biochar. Here, the dissolved Fe and Mn in the soil originating from the biochar were calculated to be 1.5 μg L^{-1} and 0.74 μg L^{-1}, respectively (S1.3, supplementary information). These concentrations were smaller by orders of magnitude than the detected values in the biochar-treated soil (dissolved Fe > 500 mg/L, dissolved Mn > 5 mg/L). Therefore, the elevated concentrations of dissolved Fe and Mn in the soils was due to the reductive dissolution of Fe/Mn(hydr)oxides (Borch et al., 2010) (Fig. 3, Fig. S3).

The same linear regression slope values (0.0004) for Hg *vs* Fe for the control and biochar-treated soils might imply that mechanisms of Fe (hydr)oxides dissolution were similar in the two soils (Fig. 4). If the mechanism of Hg mobilization was different between the control and biochar-treated soil, the regression slope values for Hg *vs* Fe should be different, which was not the case here. Therefore, the amendment of biochar appeared to promote the dissolution of Fe(hydr)oxides (also via lowering E_h), releasing more Fe as well as the associated Hg. Also, the linear regression slope value for Hg *vs* E_h was −0.001 for both, the control and biochar treatment, further demonstrating a similar mechanism controlling the mobilization of Hg in the two soils under dynamic E_h conditions (Fig. S4).

3.5.2. DOC, $SUVA_{254}$, and SO_4^{2-}

The DOC concentration (17–24 mg/L) at low E_h windows (−250 to 0 mV) exceeded those at high E_h windows (7.3–14 mg/L; +100 to +350 mV) in the control soil (Fig. 3). This phenomenon might be explained by the mobilization of organic carbon through the reductive dissolution of Fe/Mn(hydr)oxides under anoxic conditions (Rinklebe et al., 2020; Shaheen et al., 2014b). Nevertheless, the concentrations of DOC were variable in the biochar-treated soil under dynamic redox conditions (Fig. 3). For example, the lowest (7.1 mg/L) and highest (40 mg/L) values were present at E_h −300 mV and −100 mV, respectively (Fig. 3). Overall, the average concentration of DOC was increased by 56 % in the biochar treated-soil as relative to control throughout the experiment. Giving that both, control (32 mg/L) and biochar treatment (36 mg/L), had similar DOC concentrations at the beginning of experiment (initial sample), it is likely that the increased DOC concentration might be caused by biochar-promoted formation of DOC from native soil organic matter (Jiang et al., 2016), and/or microbial-mediated decomposition of small organic molecules that were bound at the surface of biochar (Yuan et al., 2017).

There was a positive correlation between the concentration of DTHg and that of DOC in the control (Table S4, $r = 0.85$), suggesting that DOC facilitated Hg migration (Jeremiason et al., 2015), as Hg binding to DOC could inhibit Hg^{2+} sorption onto surfaces of minerals (Wallschläger et al., 1996). However, no clear relation between the concentration of Hg and that of DOC was observed in the biochar treatment. This might be due to a more diverse composition of DOC in the biochar-treated soil as different sources of DOC affected mobilization of Hg differently (French et al., 2014). For example, Jiang et al. (2018) reported an opposite effect of allochthonous and autochthonous DOC on Hg availability in three Chinese lakes, since allochthonous DOC inhibited Hg availability for Hg methylation microorganisms, while autochthonous DOC stimulated MeHg formation by enhancing the activity of microbial communities.

$SUVA_{254}$ is an indicator of the aromatic moieties of DOC; a smaller value means a lower ratio of aromatic to aliphatic DOC, and vice versa (Shaheen et al., 2014a). There was no clear trend for $SUVA_{254}$ in both control and biochar treatment across the studied E_h range (Fig. 3), suggesting that $SUVA_{254}$ played a minor role in Hg mobilization under our experimental conditions.

Average sulfate concentrations were lower at E_h ranges −300 to −100 mV than 0 to +400 mV in the two soils (Fig. 3). This phenomenon might be due to microbial-mediated reduction of sulfate under reducing conditions (Burton et al., 2006; Johnston et al., 2014) and the further oxidation of reduced sulfur to sulfate under oxidizing conditions (DeLaune and Reddy, 2008). The lower average concentration of sulfate in the biochar-treated soil (32 mg/L) relative to control (43 mg/L) might be related to the promotion of microbial sulfate reduction by biochar, as biochar could deliver electron to bacteria for sulfate reduction (Sande, 2016). A negative linear correlation between the concentration of DTHg and that of sulfate in the control ($r = -0.74$, Table S4) suggested that the elevated sulfate concentration could reduce Hg mobility in the soil. This is because more sulfides could be produced through the reduction of sulfate, and it could react with Hg to form poorly soluble nano Hg_xS_y

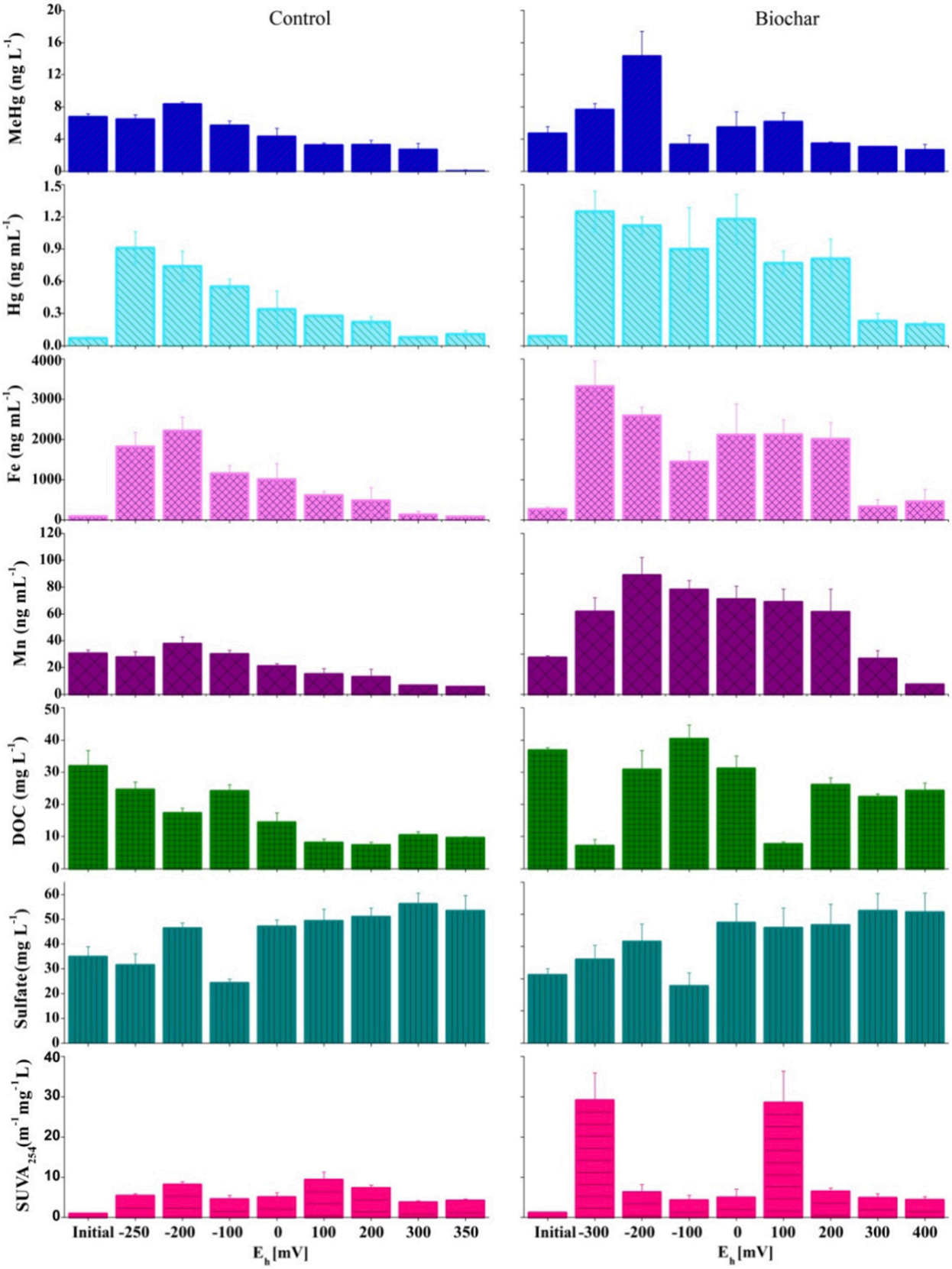

Fig. 3. The concentrations of dissolved MeHg, total Hg, Fe, Mn, dissolved organic carbon (DOC), sulfate, and SUV_{254} in the soil suspensions across the studied E_h ranges. Left: control; Right: biochar treatment.

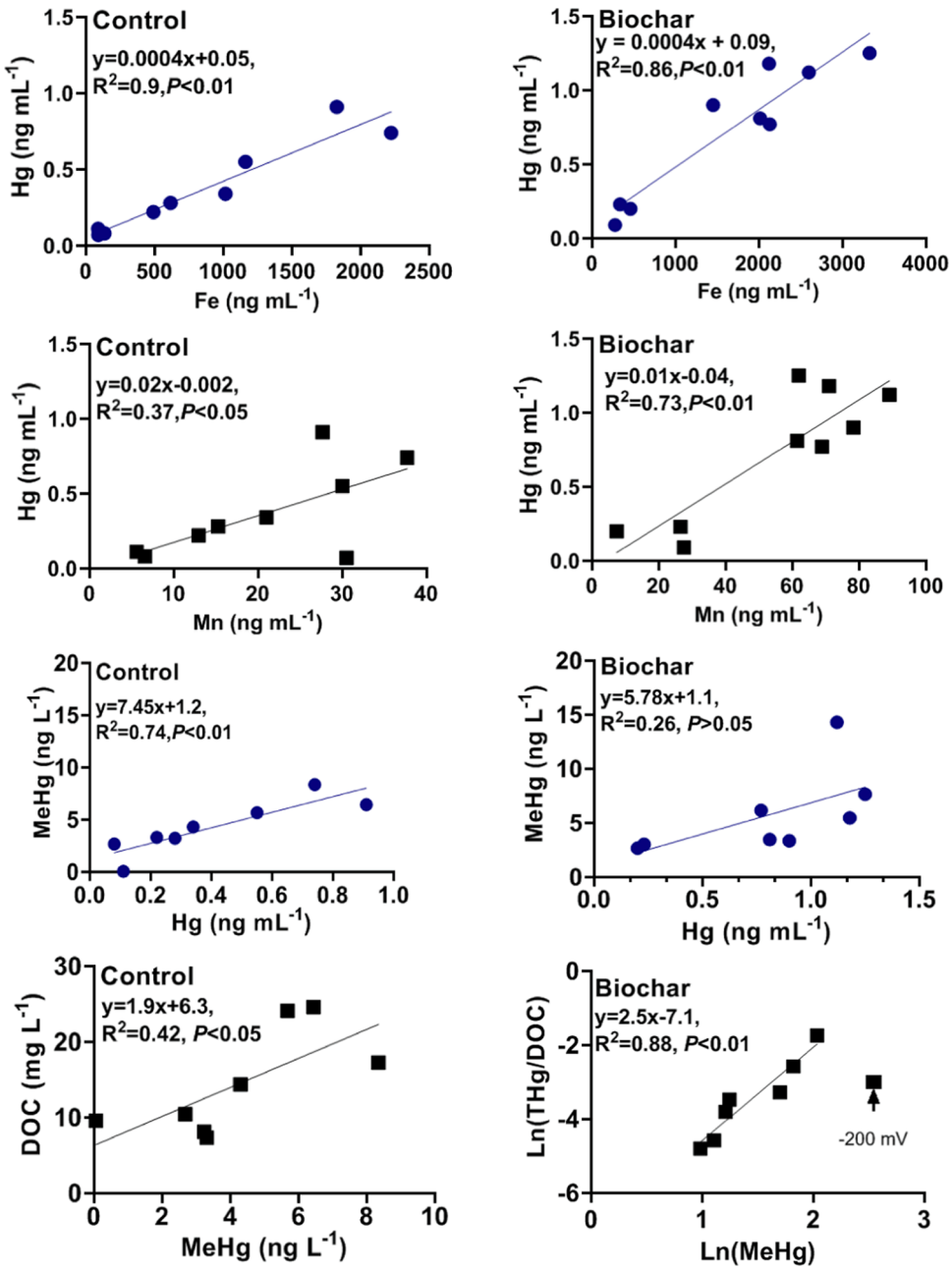

Fig. 4. Linear correlations for dissolved Fe *vs* Hg, dissolved Mn *vs* Hg, dissolved Hg *vs* MeHg, and Ln (MeHg) *vs* Ln (dissolved organic carbon (DOC))/(THg/DOC) in the soil suspensions (<0.45 μM) in the control and biochar-treated soil (n = 8). The black arrow point to the sample which was collected at E_h −200 mV.

polyclusters (Manceau et al., 2015; Pham et al., 2014).

Multivariate regression analyses of dissolved total Hg concentration with biogeochemical factors under different redox conditions showed that dissolved Fe was significantly correlated with Hg (Table S5). These results indicate that Fe was important in controlling the dissolved Hg. This is consistent with our early discussion that reductive dissolution of Fe(hydr)oxides controlled Hg mobilization. No significant correlations were observed between MeHg and biogeochemical factors (Table S5), indicating that these factors were not the dominant factors controlling the formation of MeHg. This is reasonable since MeHg was determined by both microbial activities and Hg availability (Liu et al., 2019; Hsu-Kim et al., 2018).

3.6. Molecular composition of SOM under dynamic E_h conditions

We studied the organic matter composition in the soils using Py-FIMS to understand how biochar affected soil organic matter compositions under dynamic E_h conditions (Fig. 5, Table S6).

The thermograms of total ion intensity (TII) for all samples had a unimodal shape, that showed smaller proportions of thermally labile (<400 °C) than stable (>400 °C) organic matter constituents (Figs. S5, S6). The Py-FIMS mass spectra of all samples were predominated by marker signals of carbohydrates (CHYDR; *m/z* 96, 110, 126), phenols and lignin monomers (PHLM; *m/z* 196, 208), lignin dimers (LDIM; *m/z* 372, 386, 396, 408), lipids (LIPID; *m/z* 230, 244, 298, 312, 368, 396, 408), alkylaromatics (ALKYL; *m/z* 220), Heterocyclic nitrogen compounds and nitriles (NCOMP; *m/z* 220), and free fatty acids (FATTY; *m/z* 368) (Figs. S5, S6). The marker signals in the Py-FI mass spectra were assigned to 10 compound classes of SOM, and the proportions of these compound classes are shown in Fig. 5. In the control soil, relative abundance of most compound classes (CHYDR, PHLM, LDIM, LIPID, ALKYL, NCOMP, AMID, SUBER) remained relatively constant (relative

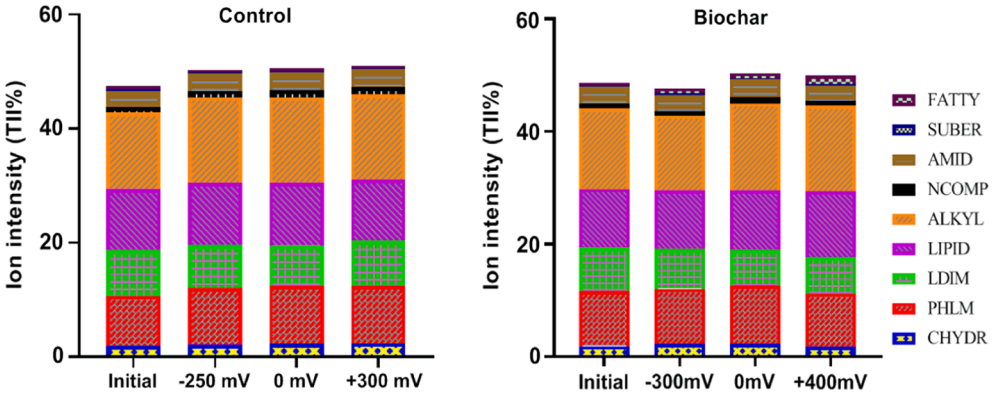

Fig. 5. Abundance of organic matter compound groups in both control and biochar-treated soil collected at different E_h windows. The unit is ion intensity (% TII). Note: CHYDR = carbohydrates; PHLM = phenols and lignin monomers; LDIM = lignin dimers; LIPID = lipids, alkanes/alkenes, fatty acids, alkyl esters, sterols; ALKYL = alkyl-aromatics; NCOMP = Heterocyclic nitrogen, nitriles; AMID = amino acids, peptides, amino sugars; SUBER = suberin; FATTY = free fatty acids (n-$C_{16:0}$ to n-$C_{34:0}$).

difference < 10 %), while most SOM groups in the biochar-treated soil (CHYDR, LIPID, ALKYL, NCOMP, AMID, SUBER, FATTY) were variable, under dynamic redox conditions (Fig. 5, Table S6).

In the biochar-treated soil, the relative abundance of LIPID, ALKYL and FATTY increased with increasing of E_h (Fig. 5, Table S6), and they were likely sourced from the byproducts from microbial biomass (e.g., alkylic C compounds (Beyer, 1995)), and from the microbial consumption of more easily decomposable compound classes (e.g., CHYDR and AMID) (Monreal and Schnitzer, 2013). Also, it is possible that LIPID, ALKYL and FATTY were resistant to microbial degradation under aerobic conditions (Wu et al., 2018). The relative abundance of CHYDR, LDIM, and SUBER as a function of E_h showed an opposite trend as compared to LIPID, ALKYL and FATTY (Fig. 5, Table S6), indicating that CHYDR, LDIM, and SUBER tended to be consumed by microorganisms under aerobic conditions. The high abundance of PHLM, NCOMP, and AMID at E_h 0 mV (Fig. 5, Table S6) is likely because the biochar-induced microbial activities resulted in complicated SOM reactions during redox changes, which needs further investigation.

To further understand the varied relative abundance of SOM compounds in both control and biochar-treated soils under dynamic E_h conditions, principal component analysis (PCA) was performed on the 177 mass signals from Py-FIMS spectra with significant differences ($P \leq 0.05$) according to Wilks' lambda (Fig. 6). The first two principal components (PCs) accounted for 71.2 % (PC1) and 11.9 % (PC2) of total variability within the data set (Fig. 6). The plot of PC1 *vs* PC2 shows a clear separation between control and biochar-treated soil. Furthermore, biochar-treated soils at different E_h ranges were separated along both PCs. Therefore, the studied biochar induced distinct alterations in the SOM composition under variable redox conditions. It was impossible to record Py-FI mass spectra of the studied biochar until heating it to 650 °C. This is due to organic matter was thermally stable, as C was present as stable graphitic structure (Fig. 1-A). Therefore, the contribution of biochar itself on the SOM compound classes is of minor importance. It has been well established that biochar could affect microbial metabolic activities, and change microbial diversity and abundance (Palansooriya et al., 2019). Giving that microorganism drives organic matter cycle in the environment, biochar can change the community of soil microorganism, and it is likely that biochar affected organic matter cycle via microorganisms (Li et al., 2012; Wang et al., 2022; Whitman et al., 2016). Therefore, we hypothesized that biochar-induced alteration of microbial community structure and activities contributed to the variation of SOM compound classes under dynamic redox conditions

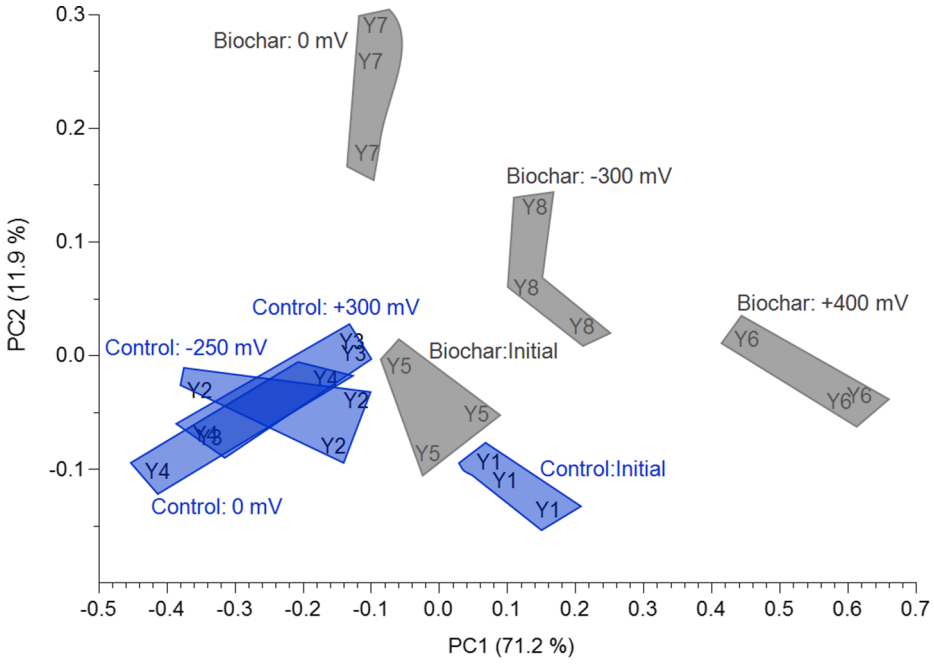

Fig. 6. Principal component (PC) analysis of the 177 *m/z* from Py-FIMS spectra of four control [Y1-initial, Y2–250 mV, Y3-+300 mV, Y4-0 mV] and four biochar-treated soil samples [Y5-Initial, Y6-+400 mV, Y7-0 mV, Y8–300 mV], with most significant differences according to Wilks' lambda. Three replicates of each soil at different redox windows were used for analysis.

(Monreal and Schnitzer, 2013; Wu et al., 2018).

3.7. Dynamic of MeHg in the soil under changing redox conditions

The MeHg concentrationin the soil solution changed as a function of E_h, and followed the order −300 to −200 mV > −100 to +100 mV > +200 to +400 mV, both in the control and biochar-treated soil (Fig. 3). The MeHg concentration in the soil solid phase showed a similar variation with the soil solution as a function of E_h in the control, while that remained relatively constant at E_h of higher than 0 mV in the biochar-treated soil (Fig. S7). The MeHg concentration decreased with rising of E_h (Fig. 3), suggesting that a lower E_h favored Hg methylation, while a higher E_h promoted MeHg demethylation. MeHg production is a microbial-mediated biogeochemical process determined by both Hg availability and microbial activities (Hsu-Kim et al., 2018). In the control, the concentration of MeHg was positively correlated with the concentration of DTHg ($R^2 = 0.74$, $P < 0.05$) (Fig. 4), suggesting that the enhanced Hg availability might account for the increase in MeHg concentration (Wang et al., 2021a). In the biochar treatment, the MeHg concentration was strongly correlated to the ratio of THg to DOC (except at −200 mV) (Fig. 4), but poorly correlated with THg concentration ($R^2 = 0.26$, $P > 0.05$).

We excluded MeHg data of −200 mV from the regression analysis for MeHg *vs* THg/DOC (Fig. 4). This was because a closer inspection of the data showed that MeHg concentration was 14 ng/L at E_h −200 mV, which was 2 to 4 times higher than that at E_h-300 (7.7 ng/L) and −100 mV (3.4 ng/L) (Fig. 3). There was an enhanced MeHg production at E_h −200 mV as relative to E_h −100 mV and −300 mV in the biochar-treated soil. To further follow this statement, we found that DOC concentration at E_h −300 mV (7.1 mg/L) was sharply increased to 31 mg/L at E_h −200 mV in the biochar-treated soil (Fig. 3). This increase would be a consequence of decomposition of organic matter via intensive anaerobic microorganism activities (Dong et al., 2014). Therefore, we predicted that higher MeHg concentration at E_h −200 mV was due to the enhanced microbial activities. As a comparison, we did not observe such significantly rising of DOC concentration at E_h −100 to 0 mV (Fig. 3). There was a positive correlation between concentrations of MeHg and THg/DOC in the control soil, but the correlation coefficient was smaller as compared to MeHg *vs* THg ($R^2 = 0.74$) (Fig. 4). This means that effect of DOC on MeHg formation in the control soil was weaker than in the biochar-treated soil.

The concentration of MeHg was lower in the control than in the biochar-treated soil at different E_h ranges (except for E_h −100 and +200 mV) (Fig. 3 and Fig. S7), suggesting the promotion of Hg methylation by biochar. Our results supported previous findings that biochar enhanced the production of MeHg in soils under anaerobic conditions (Shu et al., 2016; Zhang et al., 2019). The biochar-induced MeHg formation was mediated by both dissolved Hg and DOC (Fig. 4). High DOC concentration was unfavorable for MeHg formation in the soil with biochar amendment (Fig. 4), as biochar-induced DOC molecules might be too large to be methylated by microorganism (Benoit et al., 2001; Liu et al., 2019b). Pearson correlation analysis showed that the concentrations of MeHg in the soil were correlated significantly with the TII (total ion intensity)-proportions of LIPID ($r = 0.71$), ALKYL ($r = 0.69$), and SUBER ($r = 0.72$) (Table S7), which indicates that these SOM compound classes could have a certain effect on stimulating methylation bacterial populations and activities and/or modulate Hg availability. The LIPID, ALKYL and SUBER might affect MeHg by stimulating Hg-methylating bacterial populations through providing carbon food sources (Kainz et al., 2003; Khodadad et al., 2011). For example, it has been reported that cell wall lipids (e.g., *n*-alkanes C27–C29 and alkan-2-ones C29–C33) were available for microorganism (Meyers and Ishiwatari, 1993). Nevertheless, more studies are needed to reveal the function of LIPID, ALKYL, and SUBER in stimulating microorganism and their effects on MeHg formation.

4. Conclusions

Rice hull biochar (RHB) led to the mobilization and methylation of Hg in a paddy soil under dynamic redox conditions, while this appears particularly under strong reducing conditions. We found that the release of Hg and the formation of MeHg were E_h-dependent. The amendment of biochar to the soil resulted in a lower E_h, which promoted the reductive dissolution of Fe/Mn(hydr)oxides. The mobilization of Fe/Mn(hydr) oxides in turn was responsible for the enhanced mobilization of Hg. The used rice hull biochar seemed to affect MeHg via changing the SOM composition of soil. Our results demonstrated that one should be aware the risks caused by rice-hull derived biochar under dynamic E_h conditions (e.g., hydro-fluctuation zone), because the studied biochar may result in an enhanced releasing and methylation of Hg. Therefore, RHB is not suitable to mitigate Hg risks under dynamic redox conditions, especially under fluctuating water regime and dynamic redox conditions. These findings have implications for proper applications of RHB to mitigate Hg risks from paddy soils and consequently, reducing the risks of Hg exposure to humans by rice consumption. Future studies should further elucidate the mechanisms of different biochars on Hg mobilization and methylation aiming to identify suitable candidates to mitigate Hg risks from soils under dynamic E_h conditions.

CRediT authorship contribution statement

Ying Xing: Conceptualization, Data curation, Investigation, Methodology, Data collection, Writing – original draft. **Jianxu Wang:** Supervision, Funding acquisition, Writing – review & editing. **Christoph E.S. Kinder:** Investigation, Formal analysis. **Xing Yang:** Investigation, Formal analysis. **Michal Slaný:** Formal analysis, Validation, Writing – review & editing. **Bing Wang:** Validation, Writing – review & editing. **Hocheol Song:** Validation, Writing – review & editing. **Sabry M. Shaheen:** Data curation, Investigation, Writing – review & editing. **Peter Leinweber:** Formal analysis, Writing – review & editing. **Jörg Rinklebe:** Conceptualization, Funding acquisition, Supervision, Writing – review & editing.

Declaration of Competing Interest

The authors declare that they have no known competing financial interests or personal relationships that could have appeared to influence the work reported in this paper.

Data availability

Data will be made available on request.

Acknowledgements

We thank the Natural Science Foundation of China (42163008, 42073081, 41703116), German Alexander von Humboldt Foundation (Ref 3.5-1186537-CHN-HFST-P), Guizhou Provincial Science and Technology Project (QKHJC-ZK[2021]YB218), National and the Pioneer Hundred-Talent Program of Chinese Academy of Sciences, and the Guizhou thousand talents innovation and entrepreneurship plan (GZQ202208090) for financial support. We thank Dipl.-Chem. Claus Vandenhirtz, Laboratory of Soil- and Groundwater-Management, University of Wuppertal for technical assistance. Thanks also to Dipl.-Chem. K.-U. Eckhardt, Mass Spectrometry Laboratory, Soil Science University of Rostock for recording the Py-FI mass spectra and data evaluations.

Appendix A. Supplementary material

Supplementary data to this article can be found online at https://doi.org/10.1016/j.envint.2022.107484.

References

Amen, R., Bashir, H., Bibi, I., Shaheen, S.M., Niazi, N.K., Shahid, M., Hussain, M.M., Antoniadis, V., Shakoor, M.B., Al-Solaimani, S.G., Wang, H., Bundschuh, J., Rinklebe, J., 2020. A critical review on arsenic removal from water using biochar-based sorbents: The significance of modification and redox reactions. Chem. Eng. J. 396, 125195. https://doi.org/10.1016/j.cej.2020.125195.

Awad, Y.M., Ok, Y.S., Abrigata, J., Beiyuan, J., Beckers, F., Tsang, D.C.W., Rinklebe, J., 2018. Pine sawdust biomass and biochars at different pyrolysis temperatures change soil redox processes. Sci. Total Environ. 625, 147–154.

Beckers, F., Awad, Y.M., Beiyuan, J., Abrigata, J., Mothes, S., Tsang, D.C.W., Ok, Y.S., Rinklebe, J., 2019. Impact of biochar on mobilization, methylation, and ethylation of mercury under dynamic redox conditions in a contaminated floodplain soil. Environ. Int. 127, 276–290. https://doi.org/10.1016/j.envint.2019.03.040.

Beckers, F., Rinklebe, J., 2017. Cycling of mercury in the environment: Sources, fate, and human health implications: A review. Crit. Rev. Environ. Sci. Technol. 47 (9), 693–794.

Benoit, J.M., Mason, R.P., Gilmour, C.C., Aiken, G.R., 2001. Constants for mercury binding by dissolved organic matter isolates from the Florida Everglades. Geochim. Cosmochim. Acta 65 (24), 4445–4451.

Beyer, L., 1995. Soil microbial biomass and organic matter composition in soils under cultivation. Biol. Fertil. Soils 19 (2-3), 197–202.

Bolan, N., Hoang, S.A., Beiyuan, J., Gupta, S., Hou, D., Karakoti, A., et al., 2022. Multifunctional applications of biochar beyond carbon storage. Int. Mater. Rev. 1–51.

Borch, T., Kretzschmar, R., Kappler, A., Cappellen, P.V., Ginder-Vogel, M., Voegelin, A., Campbell, K., 2010. Biogeochemical Redox Processes and their Impact on Contaminant Dynamics. Environ. Sci. Technol. 44 (1), 15–23.

Bourke, J., Manley-Harris, M., Fushimi, C., Dowaki, K., Nunoura, T., Antal, M.J., 2007. Do all carbonized charcoals have the same chemical structure? 2. A model of the chemical structure of carbonized charcoal. Ind. Eng. Chem. Res. 46 (18), 5954–5967.

Bravo, A.G., Bouchet, S., Tolu, J., Björn, E., Mateos-Rivera, A., Bertilsson, S., 2017. Molecular composition of organic matter controls methylmercury formation in boreal lakes. Nat. Commun. 8, 14255.

Burton, E.D., Bush, R.T., Sullivan, L.A., 2006. Reduced Inorganic Sulfur Speciation in Drain Sediments from Acid Sulfate Soil Landscapes. Environ. Sci. Technol. 40 (3), 888–893.

Chen, S., Rotaru, A.-E., Shrestha, P.M., Malvankar, N.S., Liu, F., Fan, W., Nevin, K.P., Lovley, D.R., 2014. Promoting Interspecies Electron Transfer with Biochar. Sci. Rep. 4 (1) https://doi.org/10.1038/srep05019.

Cheng, H., Hill, P.W., Bastami, M.S., Jones, D.L., 2017. Biochar stimulates the decomposition of simple organic matter and suppresses the decomposition of complex organic matter in a sandy loam soil. GCB Bioenergy 9 (6), 1110–1121.

Cooper, J., Greenberg, I., Ludwig, B., Hippich, L., Fischer, D., Glaser, B., Kaiser, M., 2020. Effect of biochar and compost on soil properties and organic matter in aggregate size fractions under field conditions. Agric. Ecosyst. Environ. 295, 106882. https://doi.org/10.1016/j.agee.2020.106882.

DeLaune, R.D., Reddy, K.R., 2008. Biogeochemistry of wetlands: science and applications. CRC Press.

Dissanayake, D.K.R.P.L., Dharmakeerthi, R.S., Karunarathna, A.K., Dandeniya, W.S., 2018. Changes in structural and chemical properties of rice husk biochar co-pyrolysed with Eppawala rock phosphate under different temperatures. Trop. Agric. Res. 30 (1), 19. https://doi.org/10.4038/tar.v30i1.8275.

Dong, W.-Y., Zhang, X.-Y., Dai, X.-Q., Fu, X.-L., Yang, F.-T., Liu, X.-Y., Sun, X.-M., Wen, X.-F., Schaeffer, S., 2014. Changes in soil microbial community composition in response to fertilization of paddy soils in subtropical China. Appl. Soil Ecol. 84, 140–147.

Fang, G., Liu, C., Wang, Y., Dionysiou, D.D., Zhou, D., 2017. Photogeneration of reactive oxygen species from biochar suspension for diethyl phthalate degradation. Appl. Catal. B 214, 34–45.

Feng, X., Li, P., Qiu, G., Wang, S., Li, G., Shang, L., Meng, B.o., Jiang, H., Bai, W., Li, Z., Fu, X., 2008. Human exposure to methylmercury through rice intake in mercury mining areas, Guizhou Province, China. Environ. Sci. Technol. 42 (1), 326–332.

French, T.D., Houben, A.J., Desforges, J.-P., Kimpe, L.E., Kokelj, S.V., Poulain, A.J., Smol, J.P., Wang, X., Blais, J.M., 2014. Dissolved Organic Carbon Thresholds Affect Mercury Bioaccumulation in Arctic Lakes. Environ. Sci. Technol. 48 (6), 3162–3168.

Frohne, T., Rinklebe, J., Langer, U., Du Laing, G., Mothes, S., Wennrich, R., 2012. Biogeochemical factors affecting mercury methylation rate in two contaminated floodplain soils. Biogeosciences 9 (1), 493–507.

Guo, J., Chen, B., 2014. Insights on the Molecular Mechanism for the Recalcitrance of Biochars: Interactive Effects of Carbon and Silicon Components. Environ. Sci. Technol. 48 (16), 9103–9112.

Harris-Hellal, J., Grimaldi, M., Garnier-Zarli, E., Bousserrhine, N., 2011. Mercury mobilization by chemical and microbial iron oxide reduction in soils of French Guyana. Biogeochemistry 103 (1-3), 223–234.

Hsu-Kim, H., Eckley, C.S., Achá, D., Feng, X., Gilmour, C.C., Jonsson, S., Mitchell, C.P.J., 2018. Challenges and opportunities for managing aquatic mercury pollution in altered landscapes. Ambio 47 (2), 141–169.

Jeremiason, J.D., Portner, J.C., Aiken, G.R., Hiranaka, A.J., Dvorak, M.T., Tran, K.T., et al., 2015. Photoreduction of Hg(ii) and photodemethylation of methylmercury: the key role of thiol sites on dissolved organic matter. Environ. Sci. Processes Impacts 17, 1892–1903.

Jiang, T., Bravo, A.G., Skyllberg, U., Björn, E., Wang, D., Yan, H., Green, N.W., 2018. Influence of dissolved organic matter (DOM) characteristics on dissolved mercury (Hg) species composition in sediment porewater of lakes from southwest China. Water Res. 146, 146–158.

Jiang, X., Haddix, M.L., Cotrufo, M.F., 2016. Interactions between biochar and soil organic carbon decomposition: Effects of nitrogen and low molecular weight carbon compound addition. Soil Biol. Biochem. 100, 92–101.

Jing, Y., Zhang, Y., Han, I., Wang, P., Mei, Q., Huang, Y., 2020. Effects of different straw biochars on soil organic carbon, nitrogen, available phosphorus, and enzyme activity in paddy soil. Sci. Rep. 10, 8837.

Johnston, S.G., Burton, E.D., Aaso, T., Tuckerman, G., 2014. Sulfur, iron and carbon cycling following hydrological restoration of acidic freshwater wetlands. Chem. Geol. 371, 9–26.

Joseph, S., Cowie, A.L., Van Zwieten, L., Bolan, N., Budai, A., Buss, W., Cayuela, M.L., Graber, E.R., Ippolito, J.A., Kuzyakov, Y., Luo, Y.u., Ok, Y.S., Palansooriya, K.N., Shepherd, J., Stephens, S., Weng, Z.(., Lehmann, J., 2021. How biochar works, and when it doesn't: A review of mechanisms controlling soil and plant responses to biochar. GCB Bioenergy 13 (11), 1731–1764.

Kainz, M., Lucotte, M., Parrish, C.C., 2003. Relationships between organic matter composition and methyl mercury content of offshore and carbon-rich littoral sediments in an oligotrophic lake. Can. J. Fish. Aquat. Sci. 60 (7), 888–896.

Khodadad, C.L.M., Zimmerman, A.R., Green, S.J., Uthandi, S., Foster, J.S., 2011. Taxa-specific changes in soil microbial community composition induced by pyrogenic carbon amendments. Soil Biol. Biochem. 43 (2), 385–392.

Kim, J.-H., Kannan, A.G., Woo, H.-S., Jin, D.-G., Kim, W., Ryu, K., Kim, D.-W., 2015. A bi-functional metal-free catalyst composed of dual-doped graphene and mesoporous carbon for rechargeable lithium–oxygen batteries. J. Mater. Chem. A 3 (36), 18456–18465.

Klüpfel, L., Keiluweit, M., Kleber, M., Sander, M., 2014. Redox Properties of Plant Biomass-Derived Black Carbon (Biochar). Environ. Sci. Technol. 48 (10), 5601–5611.

Knorr, K.-H., Blodau, C., 2009. Impact of experimental drought and rewetting on redox transformations and methanogenesis in mesocosms of a northern fen soil. Soil Biol. Biochem. 41 (6), 1187–1198.

Lau, M.P., Sander, M., Gelbrecht, J., Hupfer, M., 2015. Solid phases as important electron acceptors in freshwater organic sediments. Biogeochemistry 123 (1-2), 49–61.

Leinweber, P., Jandl, G., Eckhardt, K.-U., Schulten, H.-R., Schlichting, A., Hofmann, D., 2009. Analytical Pyrolysis and Soft Ionization Mass Spectrometry. In: Senesi, N., Xing, B., Huang, P.M. (Eds.), Biophysico-chemical Processes involving Natural Nonliving Organic Matter in Environmental Systems, Wiley-IUPAC series in biophysico-chemical processes in environmental systems. Wiley, Hoboken, NJ.

Li, P., Du, B., Chan, H.M., Feng, X., 2015. Human inorganic mercury exposure, renal effects and possible pathways in Wanshan mercury mining area, China. Environ. Res. 140, 198–204.

Li, D., Sharp, J.O., Saikaly, P.E., Ali, S., Alidina, M., Alarawi, M.S., et al., 2012. Dissolved Organic Carbon Influences Microbial Community Composition and Diversity in Managed Aquifer Recharge Systems. Appl. Environ. Microbiol. 78 (19), 6819–6828.

Liang, L., Horvat, M., Feng, X., Shang, L., Li, H., Pang, P., 2004. Re-evaluation of distillation and comparison with HNO3 leaching/solvent extraction for isolation of methylmercury compounds from sediment/soil samples. Appl. Organomet. Chem. 18 (6), 264–270.

Liu, P., Ptacek, C.J., Blowes, D.W., 2019b. Mercury Complexation with Dissolved Organic Matter Released from Thirty-Six Types of Biochar. Bull. Environ. Contam. Toxicol. 103 (1), 175–180.

Liu, J., Wang, J., Ning, Y., Yang, S., Wang, P., Shaheen, S.M., Feng, X., Rinklebe, J., 2019a. Methylmercury production in a paddy soil and its uptake by rice plants as affected by different geochemical mercury pools. Environ. Int. 129, 461–469.

Liu, T., Wang, J., Feng, X., Zhang, H., Zhu, Z., Cheng, S., 2019. Spectral insight into thiosulfate-induced mercury speciation transformation in a historically polluted soil. Sci. Total Environ. 657, 938–944.

Maghsoumi, A., Brambilla, L., Castiglioni, C., Müllen, K., Tommasini, M., 2015. Overtone and combination features of G and D peaks in resonance Raman spectroscopy of the C78H26 polycyclic aromatic hydrocarbon. J. Raman Spectrosc. 46 (9), 757–764.

Manceau, A., Lemouchi, C., Enescu, M., Gaillot, A.-C., Lanson, M., Magnin, V., Glatzel, P., Poulin, B.A., Ryan, J.N., Aiken, G.R., Gautier-Luneau, I., Nagy, K.L., 2015. Formation of mercury sulfide from Hg (II)–thiolate complexes in natural organic matter. Environ. Sci. Technol. 49 (16), 9787–9796.

USEPA, 2001. Method 1630: Methyl mercury in water by distillation, aqueous ethylation, purge and trap, and CVAFS.

Meyers, P.A., Ishiwatari, R., 1993. Lacustrine organic geochemistry—an overview of indicators of organic matter sources and diagenesis in lake sediments. Org. Geochem. 20 (7), 867–900.

Monreal, C.M., Schnitzer, M., 2013. Chapter Four - The Chemistry and Biochemistry of Organic Components in the Soil Solutions of Wheat Rhizospheres. In: Sparks, D.L. (Ed.), Advances in Agronomy, Vol. 121. Academic Press, pp. 179–251.

Palansooriya, K.N., Wong, J.T.F., Hashimoto, Y., Huang, L., Rinklebe, J., Chang, S.X., Bolan, N., Wang, H., Ok, Y.S., 2019. Response of microbial communities to biochar-amended soils: a critical review. Biochar 1 (1), 3–22.

Palansooriya, K.N., Shaheen, S.M., Chen, S.S., Tsang, D.C.W., Hashimoto, Y., Hou, D., Bolan, N.S., Rinklebe, J., Ok, Y.S., 2020. Soil amendments for immobilization of potentially toxic elements in contaminated soils: A critical review. Environ. Int. 134, 105046. https://doi.org/10.1016/j.envint.2019.105046.

Pham, A.-T., Morris, A., Zhang, T., Ticknor, J., Levard, C., Hsu-Kim, H., 2014. Precipitation of nanoscale mercuric sulfides in the presence of natural organic matter: Structural properties, aggregation, and biotransformation. Geochim. Cosmochim. Acta 133, 204–215.

Porter, S.K., Scheckel, K.G., Impellitteri, C.A., Ryan, J.A., 2004. Toxic Metals in the Environment: Thermodynamic Considerations for Possible Immobilization Strategies for Pb, Cd, As, and Hg. Crit. Rev. Environ. Sci. Technol. 34 (6), 495–604.

Prietzel, J., Müller, S., Kögel-Knabner, I., Thieme, J., Jaye, C., Fischer, D., 2018. Comparison of soil organic carbon speciation using C NEXAFS and CPMAS 13C NMR spectroscopy. Sci. Total Environ. 628-629, 906–918.
Rinklebe, J., Shaheen, S.M., Frohne, T., 2016. Amendment of biochar reduces the release of toxic elements under dynamic redox conditions in a contaminated floodplain soil. Chemosphere 142, 41–47.
Rinklebe, J., Shaheen, S.M., El-Naggar, A., Wang, H., Du Laing, G., Alessi, D.S., Sik Ok, Y., 2020. Redox-induced mobilization of Ag, Sb, Sn, and Tl in the dissolved, colloidal and solid phase of a biochar-treated and un-treated mining soil. Environ. Int. 140, 105754. https://doi.org/10.1016/j.envint.2020.105754.
Sande, K., 2016. Biochar Metal Sorption and Effect on Microbial Sulfate Reduction. Master. University of Minnesota.
Savant, N., Snyder, G., Datnoff, L., 1996. Silicon management and sustainable rice production. In: Advances in Agronomy, vol. 58, Elsevier. p. 151-199.
Schaefer, J.K., Rocks, S.S., Zheng, W., Liang, L., Gu, B., Morel, F.M.M., 2011. Active transport, substrate specificity, and methylation of Hg(II) in anaerobic bacteria. Proc. Natl. Acad. Sci. 108 (21), 8714–8719.
Schmidt-Rohr, K., Mao, J.-D., Olk, D.C., 2004. Nitrogen-bonded aromatics in soil organic matter and their implications for a yield decline in intensive rice cropping. PNAS 101 (17), 6351–6354.
Schulten, H.-R., Leinweber, P., 1999. Thermal stability and composition of mineral-bound organic matter in density fractions of soil. Eur. J. Soil Sci. 50, 237–248.
Shaheen, S.M., Rinklebe, J., Frohne, T., White, J.R., DeLaune, R.D., 2014a. Biogeochemical factors governing cobalt, nickel, selenium, and vanadium dynamics in periodically flooded Egyptian North Nile Delta rice soils. Soil Sci. Soc. Am. J. 78, 1065.
Shaheen, S.M., Rinklebe, J., Rupp, H., Meissner, R., 2014b. Temporal dynamics of pore water concentrations of Cd Co, Cu, Ni, and Zn and their controlling factors in a contaminated floodplain soil assessed by undisturbed groundwater lysimeters. Environ. Pollut. 191, 223–231.
Shaheen, S.M., Antoniadis, V., Shahid, M., Yang, Y.i., Abdelrahman, H., Zhang, T., Hassan, N.E.E., Bibi, I., Niazi, N.K., Younis, S.A., Almazroui, M., Tsang, Y.F., Sarmah, A.K., Kim, K.-H., Rinklebe, J., 2022a. Sustainable applications of rice feedstock in agro-environmental and construction sectors: A global perspective. Renew. Sustain. Energy Rev. 153, 111791. https://doi.org/10.1016/j.rser.2021.111791.
Shaheen, S.M., Wang, J., Baumann, K., Ahmed, A.A., Hsu, L.-C., Liu, Y.-T., Wang, S.-L., Kühn, O., Leinweber, P., Rinklebe, J., 2022b. Stepwise redox changes alter the speciation and mobilization of phosphorus in hydromorphic soils. Chemosphere 288, 132652. https://doi.org/10.1016/j.chemosphere.2021.132652.
Shu, R., Wang, Y., Zhong, H., 2016. Biochar amendment reduced methylmercury accumulation in rice plants. J. Hazard. Mater. 313, 1–8.
Slaný, M., Jankovič, Ľ., Madejová, J., 2019. Structural characterization of organo-montmorillonites prepared from a series of primary alkylamines salts: Mid-IR and near-IR study. Appl. Clay Sci. 176, 11–20.
Slaný, M., Jankovič, Ľ., Madejová, J., 2022. Near-IR study of the impact of alkyl-ammonium and -phosphonium cations on the hydration of montmorillonite. J. Mol. Struct. 2022 (1256), 132568.
Smebye, A., Alling, V., Vogt, R.D., Gadmar, T.C., Mulder, J., Cornelissen, G., Hale, S.E., 2016. Biochar amendment to soil changes dissolved organic matter content and composition. Chemosphere 142, 100–105.
Sorrenti, G., Masiello, C.A., Dugan, B., Toselli, M., 2016. Biochar physico-chemical properties as affected by environmental exposure. Sci. Total Environ. 563-564, 237–246.
Steinbeiss, S., Gleixner, G., Antonietti, M., 2009. Effect of biochar amendment on soil carbon balance and soil microbial activity. Soil Biol. Biochem. 41 (6), 1301–1310.
Sun, N., Zhang, Y., Ding, Z., Yin, H., 2020. Progress, Main Problems and Suggestions on Accelerating the Construction of Soil pollution prevention Pilot Zone. Environ. Protect. Sci. 46, 14–20.
Wallschläger, D., Desai, M.V.M., Wilken, R.-D., 1996. The role of humic substances in the aqueous mobilization of mercury from contaminated floodplain soils. Water Air Soil Pollut. 90 (3-4), 507–520.
Wang, X.L., Fang, W.Q., Yao, Y., Liu, P., Wang, Y., Zhang, H., Zhao, H., Yang, H.G., 2015. Switching the photocatalytic activity of g-C3N4 by homogenous surface chemical modification with nitrogen residues and vacancies. RSC Adv. 5 (27), 21430–21433.
Wang, J., Feng, X., Anderson, C.W.N., Zhu, W., Yin, R., Wang, H., 2011. Mercury Distribution in the Soil-Plant-Air System at the Wanshan Mercury Mining District in Guizhou, Southwest China. Environ. Toxicol. Chem. 30 (12), 2725–2731.
Wang, J., Feng, X., Anderson, C.W.N., Xing, Y., Shang, L., 2012. Remediation of mercury contaminated sites - A review. J. Hazard. Mater. 221-222, 1–18.
Wang, S., Nan, Z., Prete, D., Ma, J., Liao, Q., Zhang, Q., 2016. Accumulation, transfer, and potential sources of mercury in the soil-wheat system under field conditions over the Loess Plateau, northwest China. Sci. Total Environ. 568, 245–252.
Wang, L., Ok, Y.S., Tsang, D.C.W., Alessi, D.S., Rinklebe, J., Mašek, O., Bolan, N.S., Hou, D., 2022. Biochar composites: Emerging trends, field successes and sustainability implications. Soil Use Manag. 38 (1), 14–38.
Wang, A.O., Ptacek, C.J., Mack, E.E., Blowes, D.W., 2021a. Impact of multiple drying and rewetting events on biochar amendments for Hg stabilization in floodplain soil from South River, VA. Chemosphere 262, 127794. https://doi.org/10.1016/j.chemosphere.2020.127794.
Wang, J., Shaheen, S.M., Swertz, A.-C., Rennert, T., Feng, X., Rinklebe, J., 2019a. Sulfur-modified organoclay promotes plant uptake and affects geochemical fractionation of mercury in a polluted floodplain soil. J. Hazard. Mater. 371, 687–693.
Wang, J., Xing, Y., Xie, Y., Meng, Y., Xia, J., Feng, X., 2019b. The use of calcium carbonate-enriched clay minerals and diammonium phosphate as novel immobilization agents for mercury remediation: Spectral investigations and field applications. Sci. Total Environ. 646, 1615–1623.
Wang, J., Shaheen, S.M., Anderson, C.W.N., Xing, Y., Liu, S., Xia, J., Feng, X., Rinklebe, J., 2020. Nanoactivated Carbon Reduces Mercury Mobility and Uptake by Oryza sativa L: Mechanistic Investigation Using Spectroscopic and Microscopic Techniques. Environ. Sci. Technol. 54 (5), 2698–2706.
Wang, J., Shaheen, S.M., Jing, M., Anderson, C.W.N., Swertz, A.-C., Wang, S.-L., Feng, X., Rinklebe, J., 2021b. Mobilization, Methylation, and Demethylation of Mercury in a Paddy Soil Under Systematic Redox Changes. Environ. Sci. Technol. 55 (14), 10133–10141.
Whitman, T., Pepe-Ranney, C., Enders, A., Koechli, C., Campbell, A., Buckley, D.H., Lehmann, J., 2016. Dynamics of microbial community composition and soil organic carbon mineralization in soil following addition of pyrogenic and fresh organic matter. ISME J. 10 (12), 2918–2930.
Wu, Y.i., Wang, S., Ning, X., Yang, M., Liu, M., Zang, F., Nan, Z., 2021. A promising amendment for the immobilization of heavy metal (loid) s in agricultural soil, northwest China. J. Soils Sediments 21 (6), 2273–2286.
Wu, X., Wu, L., Liu, Y., Zhang, P., Li, Q., Zhou, J., Hess, N.J., Hazen, T.C., Yang, W., Chakraborty, R., 2018. Microbial Interactions With Dissolved Organic Matter Drive Carbon Dynamics and Community Succession. Front. Microbiol. 9 https://doi.org/10.3389/fmicb.2018.0123410.3389/fmicb.2018.01234.s001.
Xiao, X., Chen, B., Chen, Z., Zhu, L., Schnoor, J.L., 2018. Insight into Multiple and Multilevel Structures of Biochars and Their Potential Environmental Applications: A Critical Review. Environ. Sci. Technol. 52 (9), 5027–5047.
Xing, Y., Wang, J., Shaheen, S.M., Feng, X., Chen, Z., Zhang, H., Rinklebe, J., 2019. Mitigation of mercury accumulation in rice using rice hull-derived biochar as soil amendment: A field investigation. J. Hazard. Mater. 388, 121747. https://doi.org/10.1016/j.jhazmat.2019.121747.
Xing, Y., Wang, J., Shaheen, S.M., Feng, X., Chen, Z., Zhang, H., et al., 2020. Mitigation of mercury accumulation in rice using rice hull-derived biochar as soil amendment: A field investigation. J. Hazard. Mater. 121747.
Yang, X., Shaheen, S.M., Wang, J., Hou, D., Ok, Y.S., Wang, S.-L., Wang, H., Rinklebe, J., 2022. Elucidating the redox-driven dynamic interactions between arsenic and iron-impregnated biochar in a paddy soil using geochemical and spectroscopic techniques. J. Hazard. Mater. 422, 126808. https://doi.org/10.1016/j.jhazmat.2021.126808.
Yu, K., Böhme, F., Rinklebe, J., Neue, H.-U., DeLaune, R.D., 2007. Major Biogeochemical Processes in Soils-A Microcosm Incubation from Reducing to Oxidizing Conditions. Soil Sci. Soc. Am. J. 71 (4), 1406–1417.
Yu, K., Rinklebe, J., 2011. Advancement in soil microcosm apparatus for biogeochemical research. Ecol. Eng. 37 (12), 2071–2075.
Yuan, J., Meng, J., Liang, X., E, Y., Yang, X.u., Chen, W., 2017. Organic Molecules from Biochar Leacheates Have a Positive Effect on Rice Seedling Cold Tolerance. Front. Plant Sci. 8 https://doi.org/10.3389/fpls.2017.01624.
Zhang, J., Wu, S., Xu, Z., Wang, M., Man, Y.B., Christie, P., Liang, P., Shan, S., Wong, M. H., 2019. The role of sewage sludge biochar in methylmercury formation and accumulation in rice. Chemosphere 218, 527–533.
Zhao, F.-J., Ma, Y., Zhu, Y.-G., Tang, Z., McGrath, S.P., 2015. Soil Contamination in China: Current Status and Mitigation Strategies. Environ. Sci. Technol. 49 (2), 750–759.